Petrography and environmental significance of travertine mounds in Keane Wonder Mine, Death Valley National Park

A Thesis submitted to the faculty of
San Francisco State University
In partial fulfillment of
the requirements for
the Degree

Master of Science

In

Geoscience

by

Xueran Song

San Francisco, California

August 2021

Certification of Approval

I certify that I have read Petrography and environmental significance of travertine mounds in Keane Wonder Mine, Death Valley National Park by Xueran Song, and that in my opinion this work meets the criteria for approving a thesis submitted in partial fulfillment of the requirement for the degree Master of Science in Geoscience at San Francisco State University.

Yadira Ibarra, Ph.D.
Assistant Professor,
Thesis Committee Chair

John Caskey, Ph.D.
Associate Professor

Mary Leech, Ph.D.
Professor

Petrography and environmental significance of travertine mounds in Keane Wonder Mine, Death Valley National Park

Xueran Song
San Francisco, California
2021

Spring-associated carbonate deposits that outcrop across much of the Great Basin are relicts of the region's wetter past and geomicrobiological archives of once-thriving aquatic ecosystems. Ancient travertine deposits from Keane Wonder Spring (KWST) in Death Valley National Park (DVNP) were analyzed for petrological indicators of past changes in surface water flow throughout the groundwater system. Lithofacies analyses of proximal, intermediate, and distal sections along the travertine complex were generated. The surface-exposed proximal site is dominated by aquatic plant calcification including evidence for silicification. The intermediate site represents valuable stratigraphic facies but the channel exposure resulted in extensive post-depositional alteration. Core analyses of the distal site reveal the most promising preservation potential including well-laminated textures for future geochemical analyses. Infrared Stimulated Luminesce (IRSL) dating analyses indicate a preliminary age of KWST to be ~140 ka, consistent with deposition during marine isotope stage 6 (MIS 6). Despite evidence of diagenesis at sites 1 and 2, coupled SEM-EDS and petrographic analyses reveal mineralogic controls on the preservation potential of distinct microfacies and similar work should be considered in future travertine investigations to resolve their potential as paleoenvironmental indicators.

Acknowledgements

I would like to thank my incredible advisor Dr. Yadira Ibarra for all her guidance and support. I would also like to thank Dr. Mary Leech and Dr. John Caskey for serving on my thesis committee. Big thanks to Dr. Clive Hayzelden for carrying out the SEM analyses and Dr. Sebastien Huot for assistance with the IRSL analyses. Field sample collection, reconnaissance, and sample preparation assistance was provided by K. Andrews, J. Leith, M. Mikhailova, and Dr. Laura Rademacher. Thank you to my parents for their enthusiasm and financial support which is gave me the financial means to attend graduate school. Lastly, I would like to thank my network of friends who cheered me on along the way.

Table of Contents

List of Tables

List of Figures

1. Introduction

In the coming decades, climate change is projected to reduce water availability in dryland regions worldwide (Yao et al., 2020) and the already water-stressed desert regions of the southwestern United States (Seager et al., 2014; Cook et al., 2015), making it especially important to understand the impact of drying and wetting on groundwater processes throughout the Quaternary to predict the future vulnerability of desert environments. The hyperarid climate of Death Valley, CA is an ideal place to study Quaternary terrestrial climate because its Pleistocene pluvial lakes provide indirect records of continental glacial climate corroborated by the marine isotope record (Ku et al., 1998; Lowenstein et al., 1999; Cook and Chafetz, 2017). Extensive existing terrestrial climate records from the southwest (Lowenstein et al., 1999; Machette et al., 2008; Toker et al., 2017; Van Noten et al., 2019; Wendt et al., 2020) provide the unique opportunity to calibrate a new climate archive in limestone deposits from hydrothermal spring systems known as travertine. Travertine is a chemically-precipitated continental limestone that forms around seepages and springs (Andrews et al., 1997; Hancock et al., 1999; Minissale et al., 2002; Pedley, 2009; De Filippis et al., 2012; Gandin and Capezzuoli, 2014; East, 2019). The hot spring water, which dissolves limestone underground and is supersaturated with calcium carbonate and has a high carbon dioxide partial pressure. Travertine formation is largely controlled by the amount of water, dissolved chemical components, temperature, pH, water evaporation/drying, and the topography of the spring area (e.g., slope)(Chafetz and Folk, 1984; Takashima and Kano, 2005; Gandin and Capezzuoli, 2014; Toker et al., 2017).

Many studies have used travertine deposits to reconstruct Quaternary paleoenvironments (Toker et al., 2015; Cook and Chafetz, 2017). Travertine deposits commonly occur in tectonically active areas, particularly those with arid climates, which often lack other high-resolution and continuous climate archives (Steinkampf and Werrell, 2001). Recent work on global trends in travertine deposition indicates that peaks in deposition correspond with local times of high precipitation or wet conditions (Özkul et al., 2013). However, travertine systems around the world lack detailed sedimentological analysis to fully determine the value of travertine deposits in paleoenvironmental reconstruction. Further, the complex structure and sedimentological facies, complicates the reliability of various dating methods (e.g., U/Th dating, radiocarbon dating, etc.).

In addition to their hydrological significance, the morphology of active travertine sites can also be used to understand the fossilization of the microbial communities that inhabit the spring water (Fouke, 2011). Many multiscale lithofacies associated with travertine deposition resemble early Earth deposits known as microbialites (Guo and Riding, 1994). Therefore, understanding microbial preservation in travertine has implications for improving the interpretation of early Earth sedimentary rocks that may contain evidence of life.

In this study, I investigate the lithofacies of travertine paleospring mounds of Keane Wonder Spring from the Death Valley region. The Keane Wonder Spring Travertine deposits contain well-exposed outcrops and surface features of glacial-interglacial hydrological and biogeochemical changes. The focus of this work is on the multiscale facies, petrography, and microbial and mineralogic signatures preserved in the Keane Wonder Spring Travertine (KWST)—a previously undescribed travertine spring system located in Death Valley, CA—which provides a first look at the paleoenvironmental reconstruction potential of travertine in the Death Valley region.

1.1 Paleoenvironmental interpretation from travertine deposits

Spring-associated carbonate deposits capture and preserve a record of their local depositional environment and offer an opportunity to investigate local and regional hydroclimate variability in terrestrial environments (Pentecost, 2005). Travertine deposits (Gandin and Capezzuoli, 2014) occur in tectonically active areas, which allow deeper circulation and geothermal heating of groundwater flowing through limestone bedrock (Pedley, 2009). In the southwest United States, travertine deposits have been used to develop Quaternary records of paleo groundwater flow paths and to infer water sources and semiquantitative hydrologic changes (Steinkampf et al., 1999; Machette et al., 2008; Porta and Barilaro, 2012; Della Porta et al., 2017). Thus far, most Quaternary travertine deposits that have been dated in the southwest US are from Arizona and New Mexico (Ricketts et al., 2019), with one dated deposit of lacustrine carbonates from Death Valley (Ku et al., 1998) near Keane Wonder Mine. Analyzing travertine carbonate rocks can be used to infer basin morphology and hydrology, bedrock formations, crustal structure and climate. Observing the complex microstructure of travertine, mineralogy and secondary porosity, is integral in determining depositional and postdepositional processes.

Terrestrial spring settings are known to form microbialites (Chafetz and Guidry, 1999; Gandin and Capezzuoli, 2014; Armenteros and Ghannem, 2021) and are some of the few environments on Earth where we can readily access, observe, and monitor (in situ) the lithification process in and around microbial communities on human timescales (e.g., Fouke, 2011; Arenas and Jones, 2017). Modern depositional rates of carbonate accretion in spring carbonate settings are on the order of 4 to 14 mm per year (Andrews et al., 1997; Gandin and

Capezzuoli, 2014; Arenas and Jones, 2017). These rapid calcification rates provide the unique opportunity to study the processes that control the formation of microbialites as they evolve from microbial mats into fully lithified structures in order to more accurately interpret the formation of similar morphologies in the rock record.

This project focuses on carbonate samples of travertine that were collected from Keane Wonder Mine Travertine, Death Valley, CA (Fig. 1). The purpose of this study is to describe the multiscale facies of the Keane Wonder Spring Travertine and determine the best sites for microfossil preservation and paleoenvironmental reconstruction. Characterizing the lithofacies and assessing the extent of microfossil preservation constitutes a first step towards determining the extent of preservation and paleoenvironmental archive potential of inactive travertine deposits in Death Valley. The age of deposition, mineralogy, and structure of the deposit remains unknown, but may prove to be valuable archives of the paleohydrology of the Death Valley region.

2. Environmental Setting

Travertine terraces extend for approximately 2 km^2 in the southwestern side of the Funeral Mountains in Death Valley National Park (DVNP) (Fig. 1). Keane Wonder Spring travertine (KWST) deposits consist of travertine lobes that extend for approximately 500 m on the southwestern side of the Funeral Mountains. The carbonates are at least 5 m thick, and sites with limited flow contain actively-forming pools, channels, terraces, and pustular mat, and streamer facies (Fig. 2) (Fouke, 2011; Gandin and Capezzuoli, 2014). The depositional record of the KWST remains unexplored despite its large size and conspicuous geomorphologic features.

Water temperature has been measured at various spring orifices with measurements of approximately ~25 °C. Discharging about 150 L/min a spring emerges from the Middle Member of the Crystal Spring Formation of the Pahrump Series (Troxel and Wright, 1989), a part of the Lower Clastic and Carbonate rock unit. The Middle Member of the Crystal Spring Formation is described by Troxel and Wright (1989) as mostly calcite marble. Lower clastic and carbonate rocks form the core of the northern Funeral Mountains. The spring is located near the trace of a detachment fault overlain by Tertiary rocks. The chemistry of the water, topographic setting, and the spring elevation in relation to the regional hydraulic gradient indicate the source of the water is regional groundwater flow from the northeast (Steinkampf and Werrell, 2001). The spring emerges along a possible source for deeply circulating waters that result in elevated water temperatures (up to 33.2 ºC; Bedinger and Harrill, 2012). Steinkampf and Werrell (2001) report water δ^2H and $\delta^{18}O$ of -102 ‰ and -12.95 ‰ respectively, reflecting a meteoric origin for recharge, thus validating use of KWST to reconstruct paleorecharge. The low flow of the spring, absence of other regional springs in similar hydrogeologic settings of the Funeral Mountains, and the water chemistry lead Steinkampf and Werrell (2001) to surmise that the Proterozoic core of the Funeral Mountains transmits meager regional flow to Death Valley.

3. Methods

Samples were collected from three sites along the travertine complex: proximal (sample 1), intermediate (sample 2), and distal (sample 3). The samples from the proximal site were collected from the surface (~top 20 cm) of the travertine exposure. The intermediate samples originate from an exposed mound with well-defined bedding features. The distalmost sample was collected using a portable backpack drill with a 3 cm diameter. Laboratory analyses entailed cutting and polishing rock samples to examine the mesofabric (i.e., cm-scale) textures. Scanned images of the rock slabs were taken using an EPSON high resolution scanner. Petrographic images were captured using Zeiss Axio imager.M2m petrographic microscope coupled with an Axiocam 506 color camera. The core samples were photographed with a high-resolution scanner and subsequently turned into standard thin sections for petrographic analysis. Microtextural studies, including observation of crystalline habits and biosignatures, carried out on small fragments and thin sections coated with a thin layer of carbon in the scanning electron microscope (SEM) (Sant'Anna et al., 2004), coupled with an energy dispersive spectrometer (EDS). Field-emission scanning electron microscopy of thin-section billets was performed at the San Francisco State University Electron Microscopy Facility. Specimens were mounted on standard 12 mm aluminum stubs using silver epoxy (Ted Pella), and the sides of the specimens were painted with silver paint (Ted Pella). After drying, the surfaces of the specimens to be examined were coated with 8 nm of Au/Pd using a Cressington208-HR sputter coater (Ted Pella). Specimens were stored in a vacuum chamber before imaging to facilitate outgassing before introduction into the electron-microscope sample chamber. Electron microscopy was performed using a Carl Zeiss ULTRA55 Field Emission Scanning Electron Microscope (FE-SEM).

Point counting analysis was performed using PowerPoint software on a grid where each unit area varied depending on the grain size. An average grid size of 15 x 31 units was point-counted from four different samples to identify differences in configuration. For each grid, a total of 450 points were counted to avert sampling bias (a standard amount according to Flugel

(2004)). Each point was allocated to a constituent category (spar, microspar, micrite, pore space, plants fossils, unknown, other).

Depositional chronology was constrained by luminescence dating (Aitken, 1998; Rhodes, 2011) at the Illinois State Geological Survey. A ~50 cm long core was collected using a Shaw portable core drill. The core was dissolved during the process of infrared stimulated luminescence dating. A second core was cut in half vertically and was examined petrographically at SFSU. Luminescence dating is based on the principle that quartz and orthoclase minerals (among others) have an intrinsic property of recording ambient energy, released through natural radioactivity. This clock is easily reset by a short exposure to sunlight (minutes to hours). Buried, these minerals will record the ambient energy, whenever radioisotopes of uranium 238, thorium 232, and potassium 40 experience a radioactive decay.

4. Results

4.1 Outcrop description

4.1.1 Sample 1 (proximal site)

Sample 1 was collected from the ground surface near the modern source of the spring. The surface facies at this site are covered in hollow filamentous travertine molds (approximately 1 mm in diameter and up to ~2 cm long) (Fig. 3A). On the outcrop surface, the filamentous structures align subparallel to one another and appear to intertwine in three dimensions (Fig. 3B).

4.1.2 Sample 2 (intermediate site)

Sample 2 was collected from a travertine mound where the cross section was clearly visible and well-exposed. At its thickest exposure, the travertine mound is approximately 3 m thick. The paleo flow direction can be inferred from southwest dipping beds (Fig. 4A). Sample 2 was collected from the base of the exposure (Fig. 4). Figure 4C-D highlights the presence of porous facies with vertical and elongate molds. The cross section of the travertine mounds appears heavily weathered likely due to the exposed (eroded) face (Fig. 4B). Furthermore, fossil traces that are thought to be plants or organisms can be confirmed on the cross section (Fig. 4D).

4.1.3 Sample 3 (distal site)

For sample 3, a core sample was collected from above the travertine mound using a portable drill with a 3 cm diameter (Fig. 5D). The core measures ~50 cm in length. The surface outcrop exposure of the drill site contains laminated features along adjacent eroded (exposed) areas (Fig. 5C).

4.2 Meso-scale and cross-section description

4.2.1 Sample 1 (proximal site)

Sample 1 contains distinct elongate fossil traces (approximately 1-2 mm in diameter) that are apparent on the bedding exposure (Fig. 6A). At the mm-scale in point B (Fig. 6B), there are spherical marks that resemble bubbles and elongated marks. The travertine color is generally bright and milky as compared to samples for the other sites. Cross-sections reveal the highly porous nature of the sample. Most of the pore shapes are rounded.

4.2.2 Sample 2 (intermediate site)

Travertine samples from site 2 range from black to white in color, and contain oblong pores (0.2 mm to 2 mm in diameter). White textures are probably calcite, and the brown to black colors are likely Fe-rich iron compounds and fine-grained calcite. Many of the pores contain horizontally elongated filamentous calcite raft structure (Fig. 7b). From the orientation of the cavities, it can be predicted that the depositional flow conditions were gentle.

4.2.3 Sample 3 (distal site)

Polished sections of the core sample from the distal site are displayed in Figure 8. The travertine at this site is overall white to milky in color from the cross section of the core. Some areas contain darker attributes. The dark-colored areas are mainly observed to surround the pores, and the size of the pores is larger than that of Samples 1 and 2. In addition, mm-scale laminated textures can be observed.

4.3 Thin section description and interpretation

4.3.1 Porosity

Porosity within travertines has been a topic of discussed especially since the discovery of the Pre-Salt oil fields (Chafetz and Folk, 1984; Chafetz and Guidry, 1999; Porta and Barilaro, 2012; Della Porta et al., 2017). In the KWST, porosity ranges from millimeter-sized to a few centimeter-sized (Fig. 9A, 10A). Thin section observation and outcrop analyses show that larger-scale pores and millimeter to centimeter scale, are common on the outcrop. In the thin section, the sheets and rafts commonly display abundant shelter porosity, mostly elongate in the horizontal and commonly extend up to 1 mm to 5 cm in length.

4.3.2 Calcite raft

Calcite rafts are composed of plate-like crystalline flakes (Figs. 10, A, C, D) in the center. The upper and lower surfaces of the rafts are lined with clear microcrystalline calcite. Calcite rafts are known to develop on the surface of stagnant pools, and surface degassing of CO_2 increases saturation levels, leading to calcite or aragonite precipitation (Chafetz and Folk, 1984; Arenas and Jones, 2017; Guo et al., 2017; Toker et al., 2017). It consists of individual sheets that are a few millimeters thin. These lithofacies are described as ‘paper-thin raft’ (Guo and Riding, 1994), ‘hot water ice’ (Allen et al., 1935), ‘calcite ice’ (Bargar et al., 1997), and ‘calcite rafts’ (Chafetz and Folk, 1984) in hot spring environments and in cool water cave pools (Hooke, 1999; Van Noten et al., 2019). The color of the raft is gray to black. This structure is observed in most thin sections. Sheets of calcite or aragonite cover many modern pools in active hot spring deposit.

4.3.3 Lamination structure

Laminated textures were common at sites 2 and 3. Laminae are white to black in color and some contain dense tabular micritic laminae. Laminations vary from parallel, horizontal, to more generally slightly undulating. Some laminated sections produce planar pores parallel to the lamination. The thickness of the individual thin layers varies between 0.1 mm and 1 mm. Laminae have transient boundaries and are characterized by color changes. The density of the stack is probably caused by seasonal changes and algae filaments. The whitish layer may be predominantly inorganically precipitated, while the dark layer corresponds to the micrite (Fig. 11C). The dark thin layer is porous, while the whitish thin layer is less porous, denser and more compact. This structure is present in flakes of samples taken from the core of the study area and is probably present in all travertine thin sections (Fig. 11A).

4.4 Site 2 point count results

Percent composition of each thin section based on point count data from Table 1. The travertine of the carbonate rock sample A from site 1 was composed of 17% micrite, 48% microspar, 8% spar, 23% pore space, 3% fossils. Sample B was composed of 29% micrite, 41% microspar, 4% spar, 9% pore space, 17% fossils. Sample C was composed of 12% micrite, 65% microspar, 11% spar, 5% pore space, 5% fossils. Sample D was composed of 27% micrite, 42% microspar, 9% spar, 18% pore space, 2% fossils. The average of samples A to D was composed of 21% micrite, 49% microspar, 8% spar, 14% pore space, 7% fossils.

These results indicate that microspar comprises approximately half of travertine samples investigated, followed by micrite, spar, and pore space. The fossil proportion of sample B is higher than the other three because of the high proportion of calcite raft.

4.5 IRSL Results

A depositional age determined by IRSL resulted in 141 ± 14 ka on a section of the Keane Wonder Mine core (Fig. 8). The age distribution is expressed as a radial plot (Fig. 12). The best age estimate is 141 ± 14 ka (1 sigma). Each circle on the radial plot represents the age and uncertainty, for a single aliquot. The age is read on the arc axis, by drawing a straight line from (0, 0), passing through a circle and intersecting the radial axis (log scale). The (0, 0) coordinate corresponds to a 0 standardized estimate (y-axis) and 0 precision (x-axis). The uncertainty is read on the horizontal axis, by drawing a perpendicular line reaching a circle. Hence, two aliquots, having the same age, but with different uncertainty, will lay on the same straight line (from (0, 0) to the radial axis). The aliquot with the smaller uncertainty (higher precision) will be closer to the arc. Values (filled circles) within the light grey shaded band are consistent (at 2σ) with the weighted mean (Central Age Model). A cluster of aliquots within this shaded band expresses confidence that we have a population of grains consistent with a single age.

4.6 SEM-EDS Results

A part of sample 1 (proximal site) was observed by SEM–EDS to determine the chemical role of microfossil preservation (Fig. 13). Figure 14 illustrates a strong the distribution of Mg and Si associated with the interpreted macrophyte (plant) fossils and an inverse correlation with Ca and S. The distribution of Sr and O is uniform across the sampled region. In Figure 15, the elements were measured by focusing on the needle spar secondary (diagenetic) crystal, which contain elevated Sr. Figure 16, focuses on the plant (likely root) fossils, and reveals a strong Si elemental measurement, suggesting the fossil preservation is likely attributed to silicification. In Figure 17, the elemental measurement on a part that seems to be a cross-section of a plant stem contains elevated Mg and Si. Ca and Sr are detected inside the outline of the cell (likely infill cement), and O is distributed throughout. This agrees with the elemental spectrum results in Figure 18. The SEM-EDS results indicate that although the macrophyte fossils have largely decayed (thus leaving behind the filamentous molds), their former presence impacts the preservation of the remaining cellular features in the form of silicification.

5. Discussion

Carbonate deposition in a hot spring systems reflect the characteristics of the geothermal/tectonic regime that provides warm to hot hypersaturated alkaline–sulfate waters resulting from a deep hydrothermal circulation into a volcanic and/or carbonate/sulfate-rich bedrock. The hot spring system is a complex environment governed by physicochemical and hydrodynamic proprieties that, when combined, make the thermal depositional conditions different from those of other marine and continental carbonates. Keane Wonder Mine spring emerges from the Upper Proterozoic and Lower Cambrian rocks of the lower plate of the Detachment Fault in contact with the upper plate of Tertiary sedimentary rocks (Bedinger and Harrill, 2012). Keane Wonder Spring shows an example where interconnected faults and fault zones on the lower plate of a fault provide a conduit for groundwater flow. The observations of this study are significant because they provide a first look at the textural differences between three different facies along the travertine depositional transect to use in future studies that reconstruct Pleistocene depositional conditions.

5.1 Comparison of the three sites

The meso- to microfacies of the three sample locations described here show some common characteristics despite their distinct locations along the travertine mound transect. Samples from site 2 and 3 are characterized by their mm-scale laminations, which can be evidence of periodic changes in sedimentation. Variations in lamination thickness can be caused by purely physical factors such as flood events and other weather patterns (Capezzuoli et al., 2014). Often, laminae are directly or indirectly related to biological activity as it may reflect other periodicities such as day length and seasonal rainfall. Laminations can exist on a variety of scales so that travertine can keep a detailed record of past history (Toker et al., 2015). The laminae can be flat, wavy, or regularly wavy (corrugated). Since no evidence of biological activity could be confirmed in this study, it is considered that the laminated structure of KWST was probably constructed by physical factors and changes in sedimentation.

As observed in the field, the measured sections of Keane Wonder Mine Travertine Sample 2 are laterally related to each other (Fig. 4, A). These m-scale exposures provide the means for direct stratigraphic facies observations. However, the bedding exposures also limit the preservation potential of the laminated facies. The petrographic results from this site show extensive diagenetic Fe-staining associated with secondary cement formation (Fig. 10). Other structures commonly found in travertine, such as shrub-flat phase and laminated structures were also observed (Fig. 10). Travertine with similar microfacies can form in shallow lake and pool environments fed by hot spring water such as in New Mexico, USA (Cook and Chafetz, 2017), Italy (Minissale et al., 2002), and Turkey (Toker et al., 2015). There are few travertines without layers, and layered structures are often the most obvious structural feature of rocks. It is important to note that despite the well-bedded nature of the travertine facies exposures like at site 2, the samples need to be investigated petrographically for diagenetic assessment.

In contrast to samples from site 1 and 2, the core sample at the distal site exhibits the longest continuous facies preservation, lamination textures, and the least diagenetic Fe-staining and pore space. These observations suggest that secondary dissolution and cementation predominately affects exposed outcrops like samples from site 1 and 2. Future samples to be used in seeking depositional geochemical information from ancient travertine sites need to consider the effects of diagenesis more closely and can used as a means to narrow down sample selection.

5.1.1 Facies interpretation

The microfacies described here bear strong resemblance to travertine deposits in New Mexico that have two depositional systems: sheets and rafts, and shrub-flat phase (Guo et al., 2017). Tivoli travertine, on the other hand, contains shrub fauna, terrace mound, and slope mound fauna (Guo and Riding, 1994; Gandin and Capezzuoli, 2014). Stacks are common sedimentary structures, usually interpreted as the effects of changes in water composition, temperature, and biological activity in static pools (Pentecost et al., 2005) and are produced by alternating and continuous layers of crystal layers of different sizes. The change in density and color is due to the seasonal growth of algae and bacteria. The dark color observed at the stacking level correlates with the high oxide content of Fe. These horizontally layered travertines can be interpreted as being deposited by a slow, continuous laminar flow in the depression filling. The root structure stabilizes the sediments, and these plant materials are covered with fine calcium carbonate to fill the space (Guo and Riding, 1994).

Sheets and calcite rafts are common components of active modern travertine sites, as well as at KWST. They are formed as surface deposits of travertine and as cavities within these deposits. At active travertine sites, they form in highly supersaturated water that moves slowly from relatively quiet locations (e.g., pools). Mammoth Hot Springs (Fig. 13) in Yellowstone National Park, Wyoming, USA contains many examples of actively-forming raft structures (Chafetz and Folk, 1984). These sheets and rafts mean rapid precipitation as surface deposits where CO_2 is degassed (Toker et al., 2015; Cook and Chafetz, 2017; Guo et al., 2017; Van Noten et al., 2019). In other active areas where travertine precipitates, it has been observed that sheets form on the surface of the pool at a depth of centimeters within 10 to 15 minutes after the surface has cleared the previous precipitate (Chafetz and Guidry, 1999; Toker et al., 2017). Sheets and rafts, which become heavier due to increased mineral sedimentation, generally sink a few centimeters below, mostly in contact with supersaturated water, or when the water surface is disturbed by wind or rainfall. After sinking to the surface of water deposits, they develop shelter porosity beneath them (Fig. 9, AD). There is no active deep pools in the current KWST, and no thin floating sheets can be seen. From the thin section observations, the hot spring activity was probably more active in the past at KWMT and contained several pool facies throughout. The sites that contain the sheet and calcite raft structures represent areas that once hosted travertine pools and is evidence of accelerated groundwater flow during travertine formation.

Travertine microfabric is dependent on the deposition environment and is affected by common physicochemical and biological conditions during $CaCO_3$ nucleation and crystal growth (De Boever et al., 2017). Immediately after travertine deposits, additional diagenesis frequently occurs. The most important texture components of travertine are micrite (mud), sparite, and more complex dendrites. All of these may constitute the original or primary fabric of travertine, but secondary fabrics resulting from diagenesis are usually present and not always reliably distinguishable (Takashima and Kano, 2005).

In Keane Wonder Mine travertine, recrystallization of sparite (samples 2 and 3) and recrystallization of needle-shaped aragonite (sample 1) can be confirmed mainly in the pores. Crystallization of samples 1 and 3 is considered to be a secondary structure after deposition, and sample 1 (Fig. 9 B) crystallizes from top to bottom in the pores. Spar fabrics in other pores can be observed in the same direction suggesting growth under the influence of gravity. On the other hand, in sample 2 (Fig. 10 C), needle-like crystals of aragonite are also observed in the pores, and it can be seen that crystallization is also proceeding from the upper part in the pores. Shrub structures can be observed in all samples. Shrub structures are often interpreted as calcification associated with bacteria and fungi (Cook and Chafetz, 2017), however unequivocal biological activity (e.g., microfossils) were not observed in the samples investigated in this study.

5.2 IRSL Interpretation

IRSL dating of a core of travertine from Keane Wonder Mine travertine site 3 places a growth pulse of travertine at 141 ± 14 ka. This date corroborates regional hydroclimate data (Ku et al., 1998; Lowenstein et al., 1999; Steinkampf et al., 1999; Owen et al., 2011).

5.2.1 Comparison to local paleohydroclimate records

IRSL dating of the core from the distal site reveals a preliminary depositional age of 141 ± 14 ka, which agrees with what we know about the timing of travertine deposition worldwide (during interglacial periods (Ricketts et al., 2019)). This date corroborates regional hydroclimate data (Ku et al., 1998; Lowenstein et al., 1999; Steinkampf et al., 1999; Owen et al., 2011) that suggest Marine Isotope Stage 6 (MIS6) was a pluvial period, however, more dates are needed to refine the current age interpretation and identify other potential travertine aggradation periods.

Despite the limited age results presented here, it is interesting to note that data from a 200 k.y. paleoclimate record of a salt core from Death Valley (DV93-1), records major lacustrine phases in Death Valley from 10 ka to 35 ka and 120 ka to 186 ka (Lowenstein et al., 1999). Of these two wet phases in Death Valley, data from Lowenstein et al., (1999) reveal that the penultimate period had deeper and longer lasting lakes than the last glacial lake. Other data from the Great Basin is supported by radiometric dating of ancient shoreline from Lake Manly and Lake Owens in the southwestern United States, including the location of Pleistocene lakes. Evidence of a combination of ancient lakes and alpine glaciers shows that the humidity of southwestern United States during MIS6 in Death Valley, was higher than in the last glacial period (Steinkampf and Werrell, 2001). The lack of a last glacial maximum age of travertine growth in this study may be attributed to several reasons having to do with the limited sample collection, erosion, or lobe switching associated with travertine deposition. Future work on dating of proximal sites near the modern spring orifice will further refine the timing of additional significant travertine aggradation periods to improve and better resolve the timing of climate changes in the Death Valley region.

6. Conclusions

Proximal, intermediate, and distal travertine lithofacies analyses of Keane Wonder Spring Travertine (KWST) record local processes of sedimentation. The surface-exposed proximal site is dominated by aquatic plant calcification including evidence for silicification. The intermediate site represents valuable stratigraphic facies but the channel exposure resulted in extensive post-depositional alteration. Core analyses of the distal site reveal the most promising preservation potential including well-laminated textures for future geochemical analyses. IRSL analyses indicate a preliminary age of Keane Wonder Mine Travertine to be ~140 ka, consistent with deposition during marine isotope stage 6 (MIS 6). Despite evidence of diagenesis at sites 1 and 2, coupled SEM-EDS and petrographic analyses reveal mineralogic controls on the preservation potential of distinct microfacies and similar work should be considered in future travertine investigations to resolve their potential as paleoenvironmental indicators.

7. Future Work

Due to the COVID-19 pandemic, some analyses were excluded from this study but should be considered for future work. Additional dating of core samples using luminescence dating and other techniques will improve the timeline of changes observed in textural analyses presented here. The chronologies can be used to interpret the hydrogeological history of the study area. Additional coupled SEM-EDS analyses will clarify the extent to which microorganisms are preserved in distinct facies along the travertine depositional system. Finally, pollen is a valuable proxy that can help corroborate existing pollen records and broaden paleoclimate records in the region. The distribution of palynomorphs reveals patterns of paleoclimate conditions such as humidity, plant diversity, and relative abundance palynofloral changes through time as matched to known depositional periods and local stratigraphy.

Figure 1. Geologic Map of Keane Wonder Mine Travertine, CA

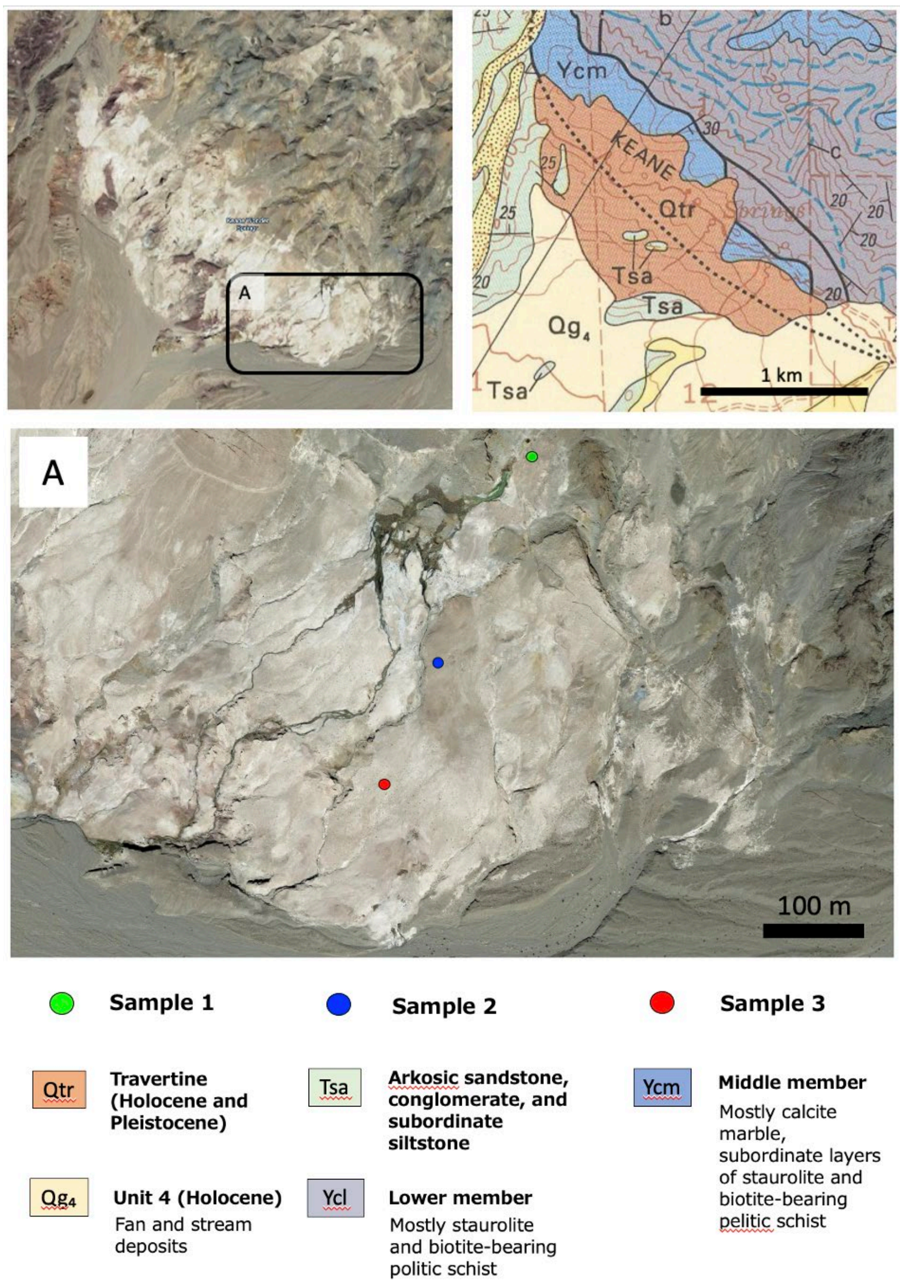

Figure 1. Geologic map of The Central & Northern Funeral Mountains & Adjacent areas, Death Valley Region, Southern California. Includes locations of travertine deposits noted in this study. Map adapted from Wright & Troxel, 1993.

Figure 2. Channels, terraces, and pustular mat, and streamer facies in KWST

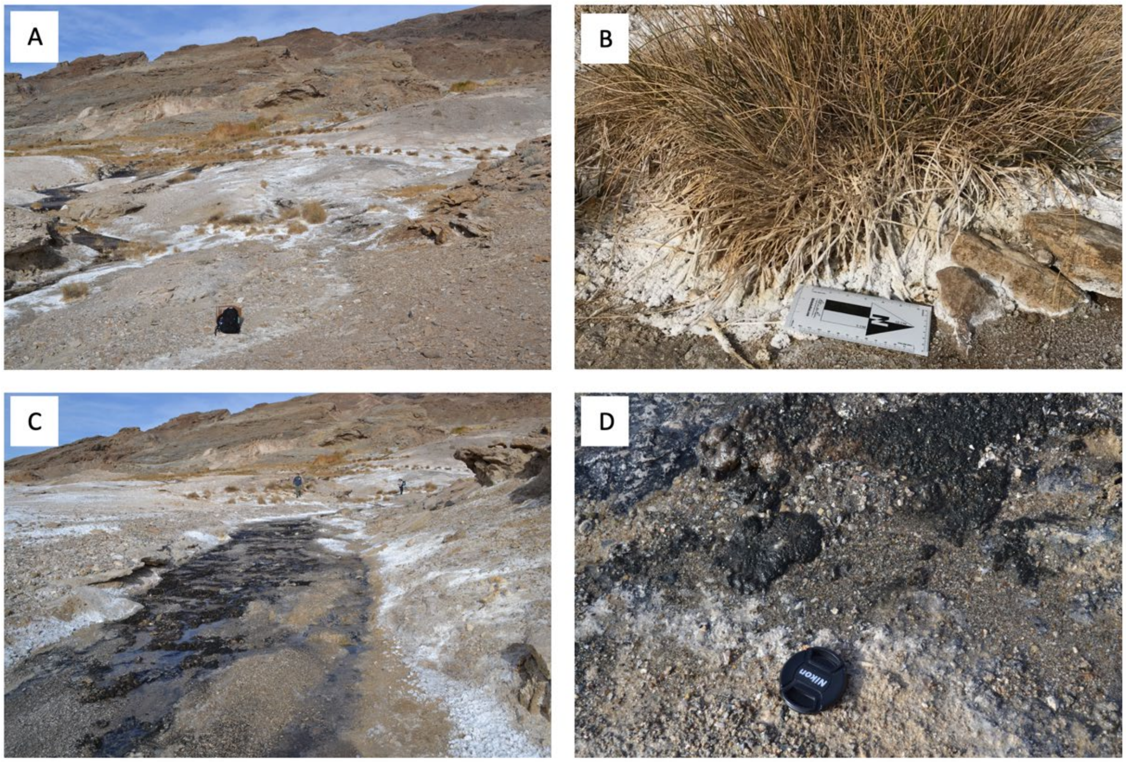

Figure 2. Actively forming channels (A), terraces, and pustular mat (C, D), and plants (B) from KWST.

Figure 3. Outcrops of Sample 1 (proximal site)

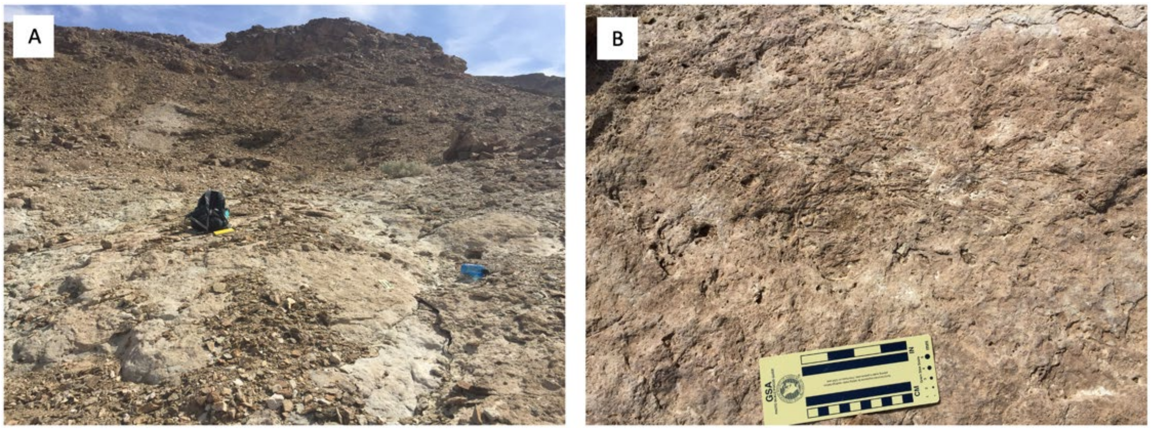

Figure 3. Outcrops (A, B), sample 1 collected point and fossil traces (B) from KWST.

Figure 4. Outcrops of Sample 2 (intermediate site)

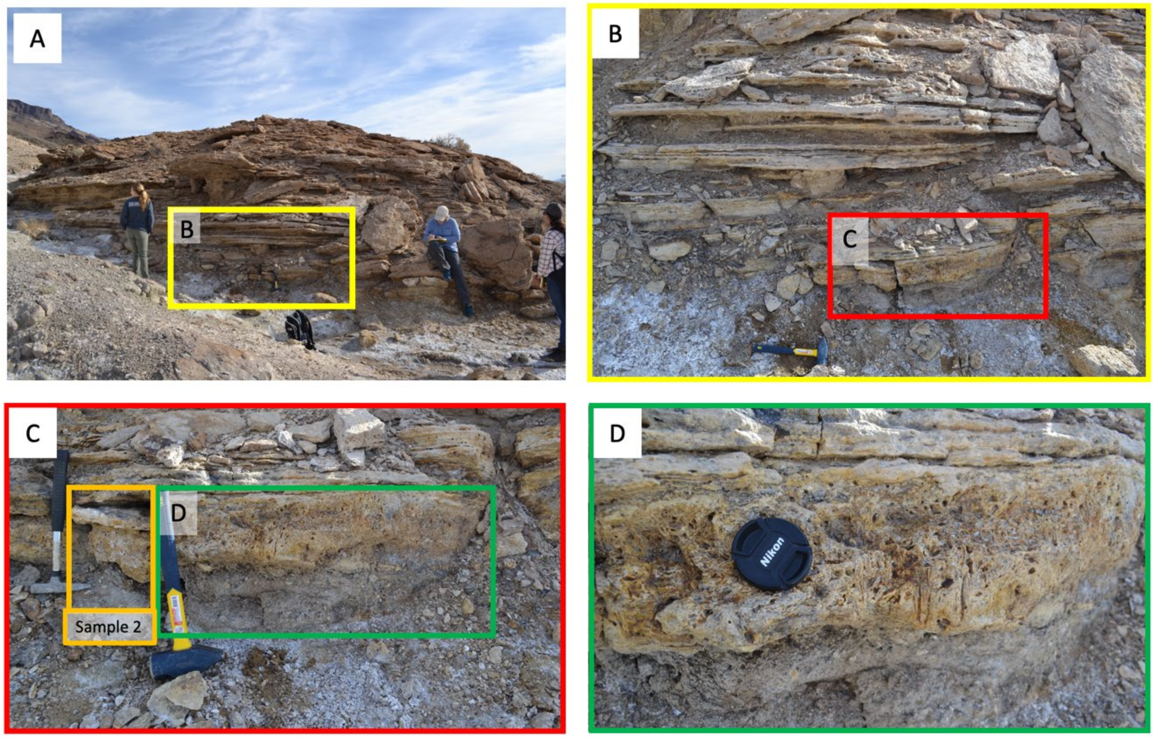

Figure 4. Outcrops (A, B, C, D), sample 2 (proximal site) collected point (C), fossil traces (D) from KWST.

Figure 5. Outcrops of Sample 3 (distal site)

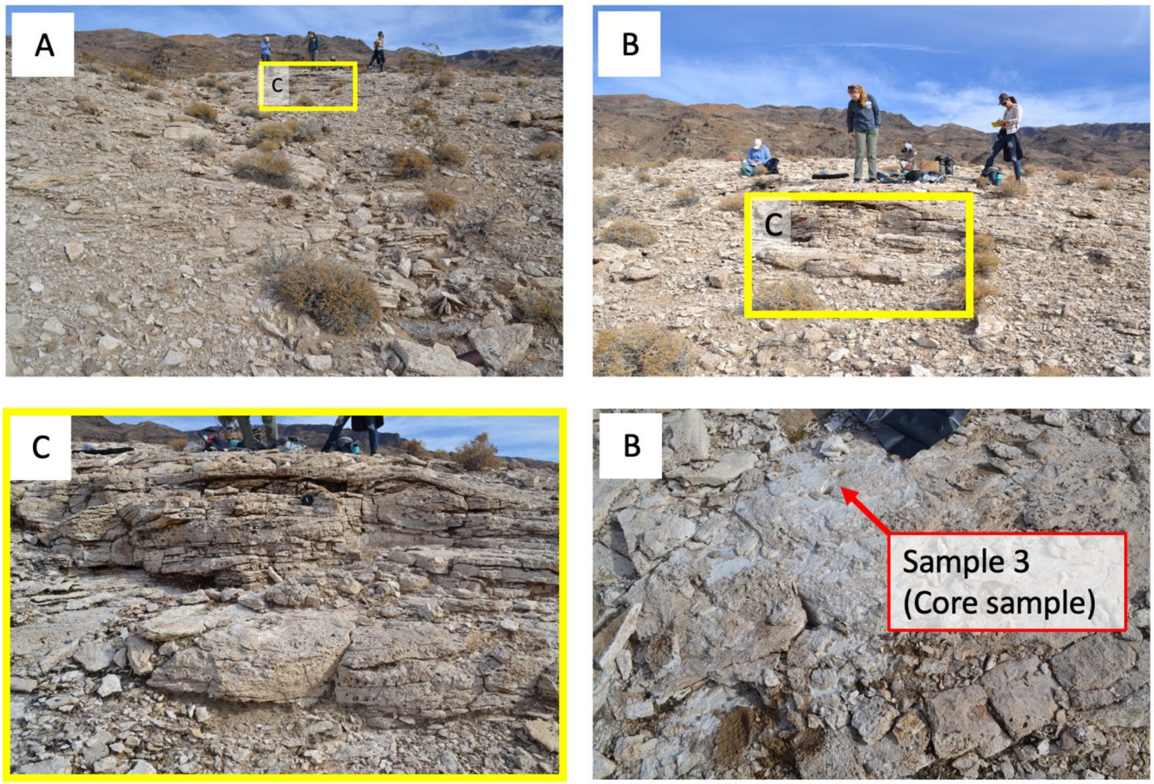

Figure 5. Outcrops (A, B, C, D), Lamination structure (C), drilling core sample at Keane Wonder Spring. Samples were drilled and placed in dark sample bags to avoid sunlight exposure (B) sample 3 collected point (D) from KWST.

Figure 6. Meso-scale and cross-section of Sample 1 (proximal site)

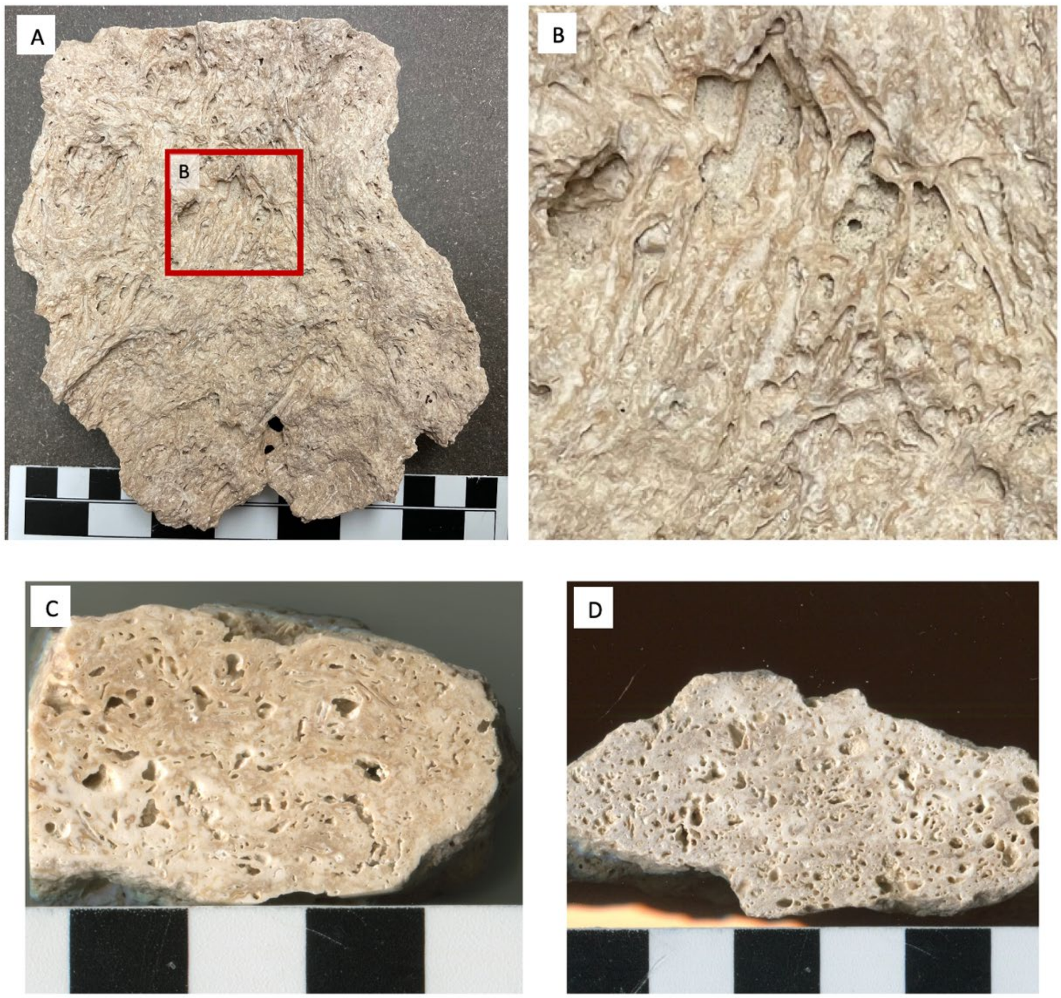

Figure 6. Meso-scale (A), spherical marks like bubbles and elongated marks (B), Cross-section (C, D), sample 1 (proximal site) collected from KWST.

Figure 7. Meso-scale and cross-section of Sample 2 (intermediate site)

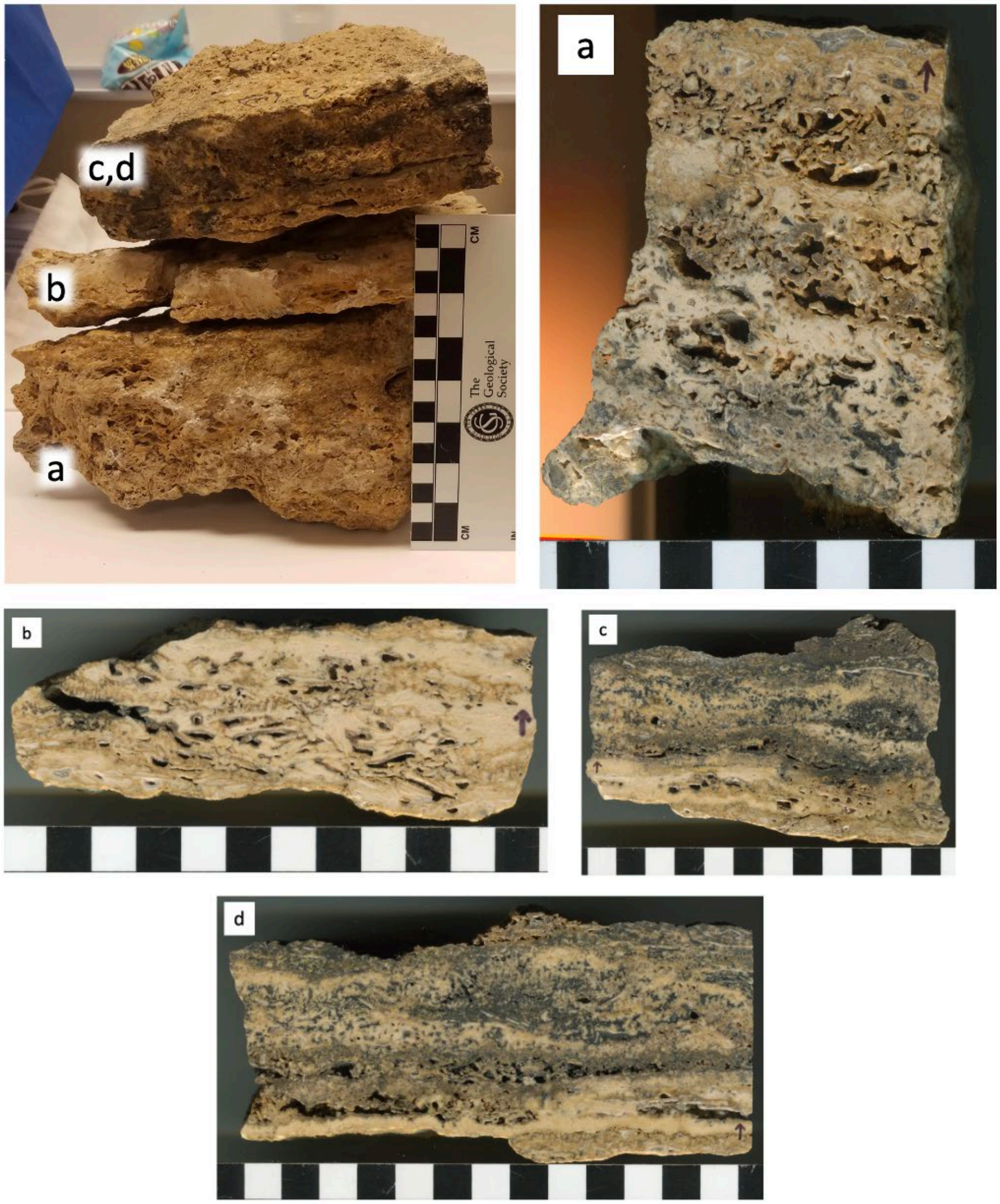

Figure 7. Meso-scale (A), Cross-section (a, b, c, d), Lamination structure (b), sample 2 (intermediate site) collected from KWST.

Figure 8. Meso-scale and cross-section of Sample 3 (distal site)

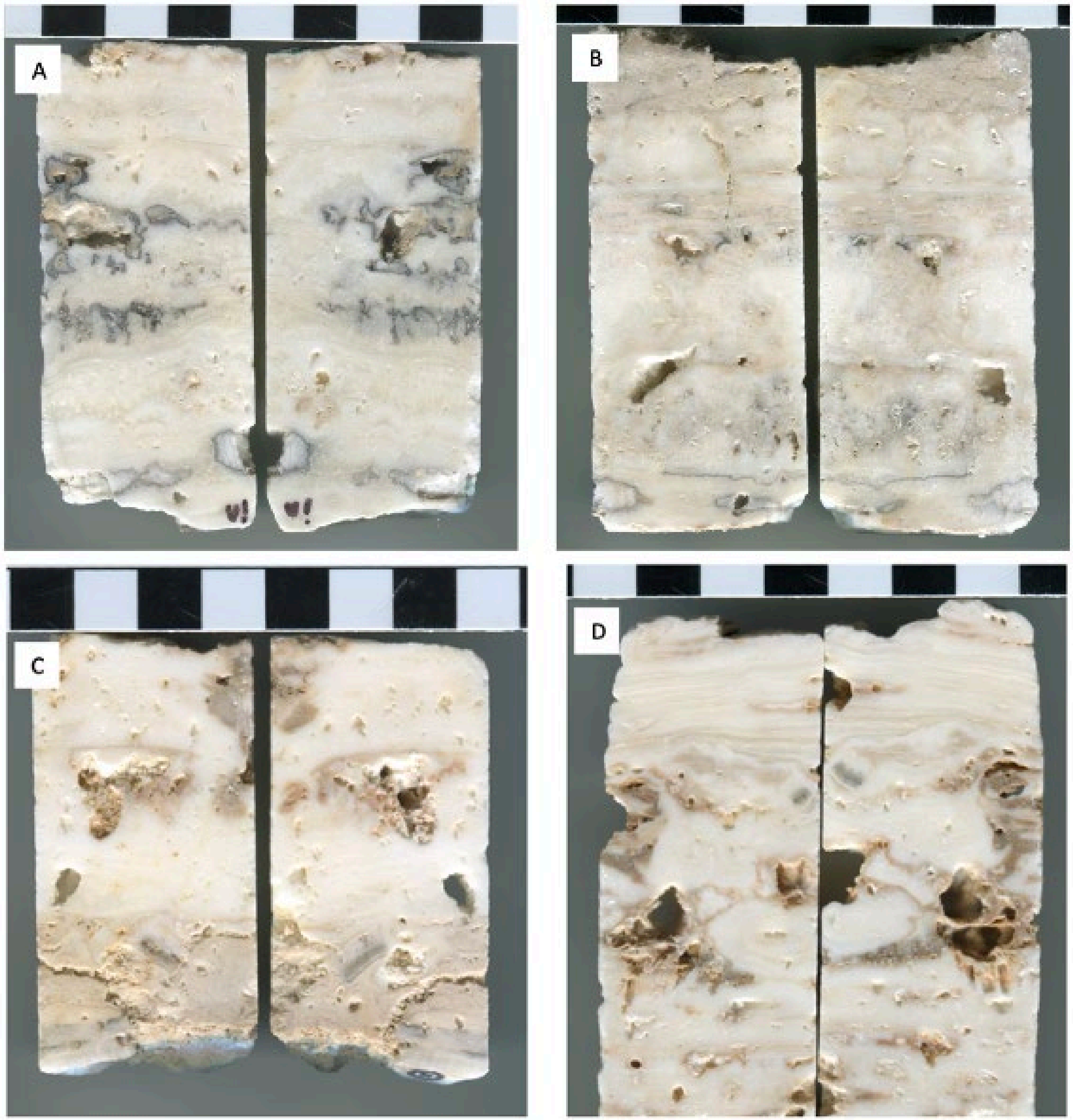

Figure 8. Scanned photos of the carbonate cross-section core sample (A, B, C, D), sample 3 (distal site) collected from KWST.

Figure 9. Thin section of Sample 1 (proximal site)

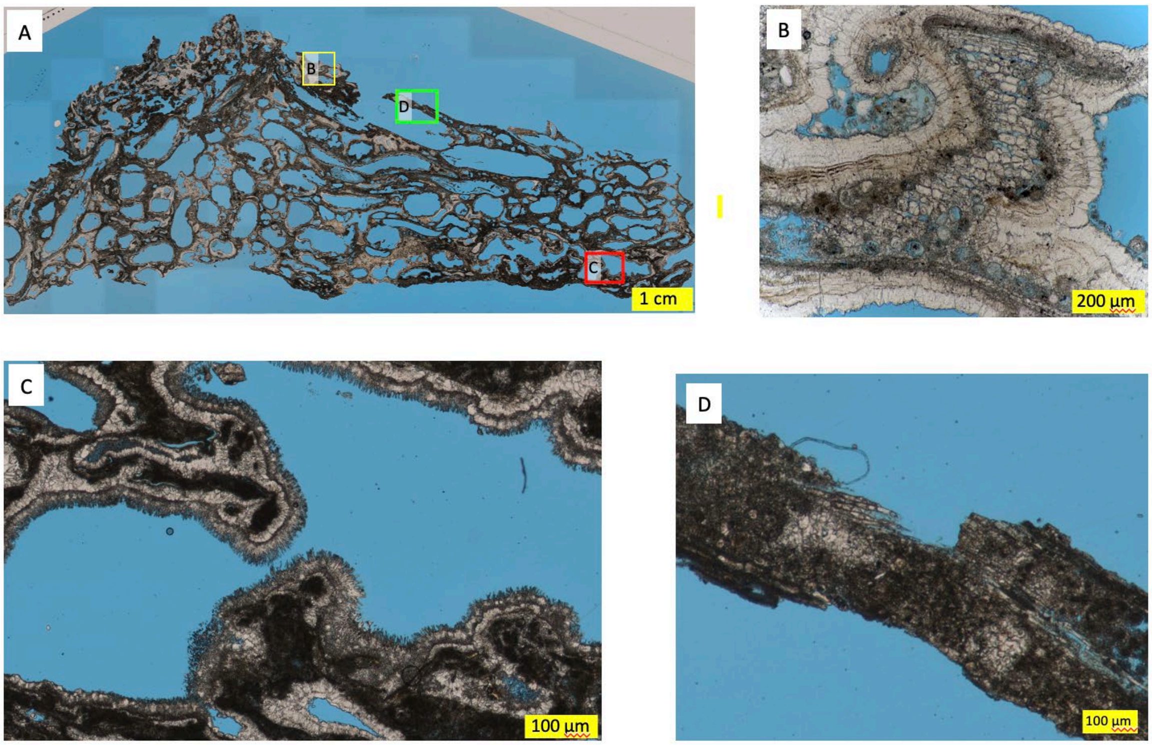

Figure 9. Thin section of sample 1 (A, B, C, D), cross section of aquatic terrestrial plants (B, D), diagenetic fibrous needles form isopachously in the pores (C).

Figure 10. Thin section of Sample 2 (intermediate site)

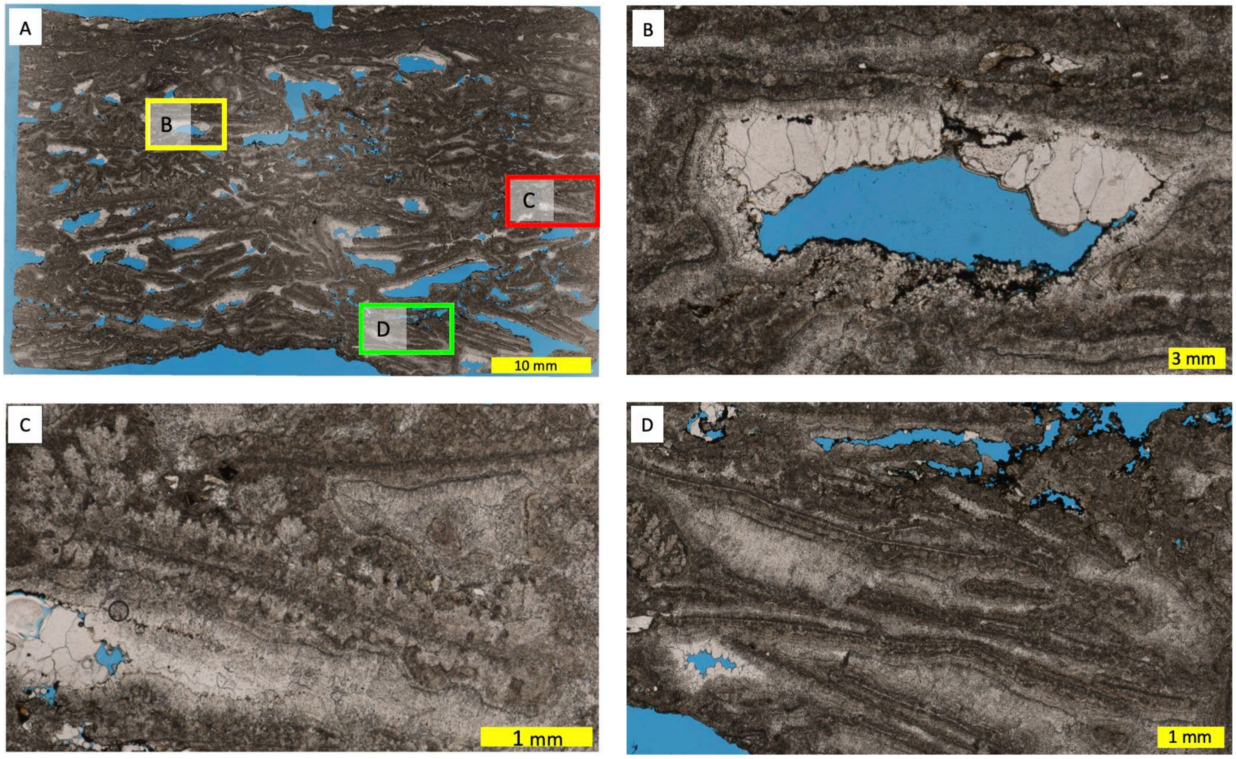

Figure 10. Thin section of sample 2 (A, B, C, D), difference in crystal growth depending on the vertical position in the porous (B), micritic rafts surrounded by calcite spar (C), most of the rafts exhibit precipitation of overgrowths on both their lower and upper surfaces (D).

Figure 11. Thin section of Sample 3 (distal site)

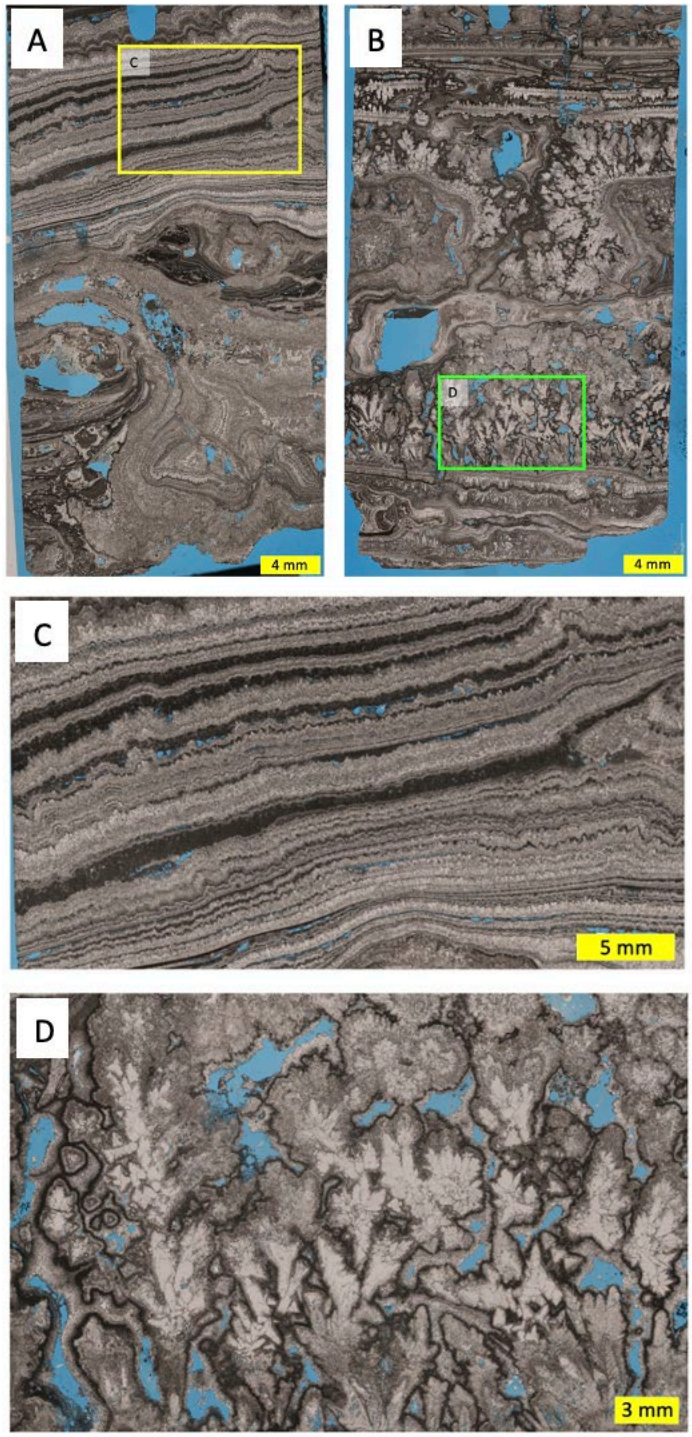

Figure 11. Thin section of sample 3 (A, B, C, D), lamination structure (C), Shrubs structure (Feather-like crystals) (D).

Figure 12. IRSL dating of Keane Wonder Mine travertine in Death Valley

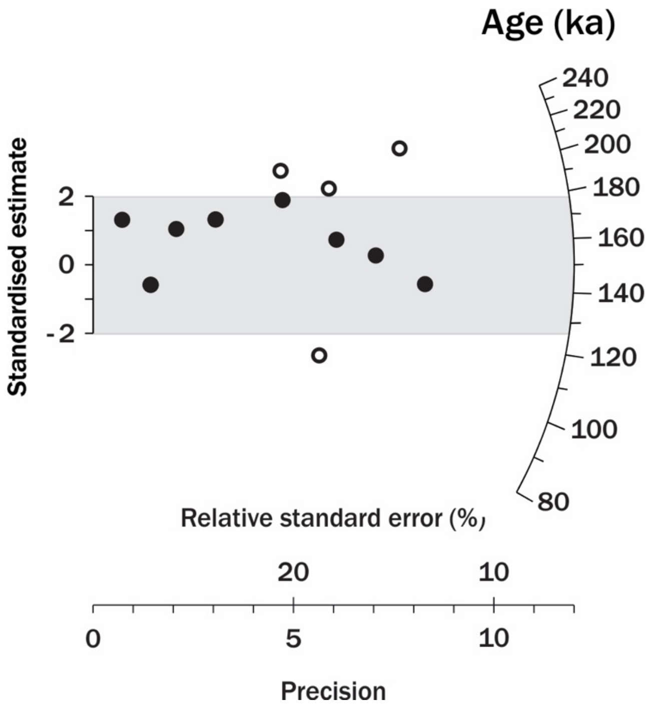

Figure 12. Preliminary age distribution, as a radial plot, for Keane Wonder Spring Travertine sample.

Figure 13. Thin section (Sample 1 (proximal site) of KWST in Death Valley

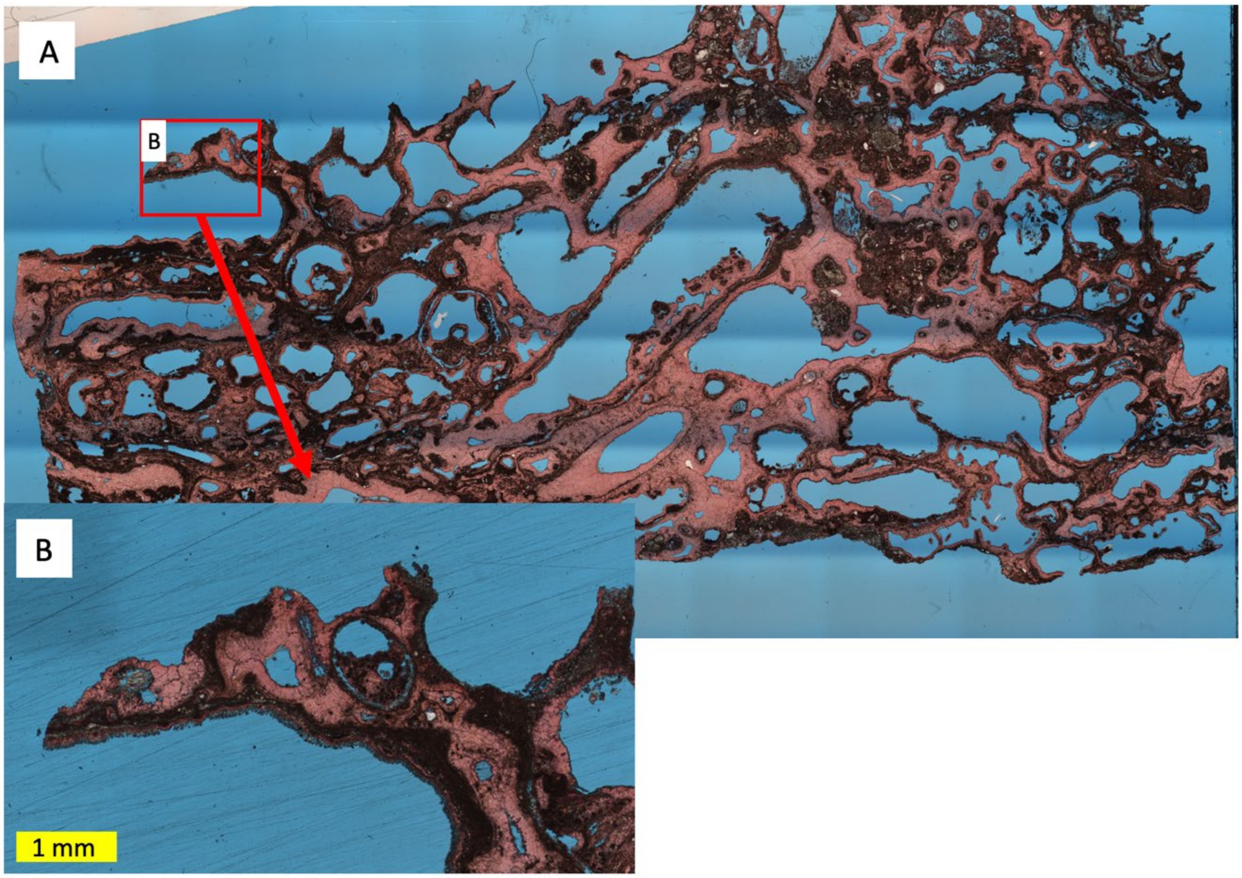

Figure 13. Sample 1 (proximal site) thin section A. Points used for SEM observation B.

Figure 14. SEM image and elemental distribution of KWST (Sample 1)

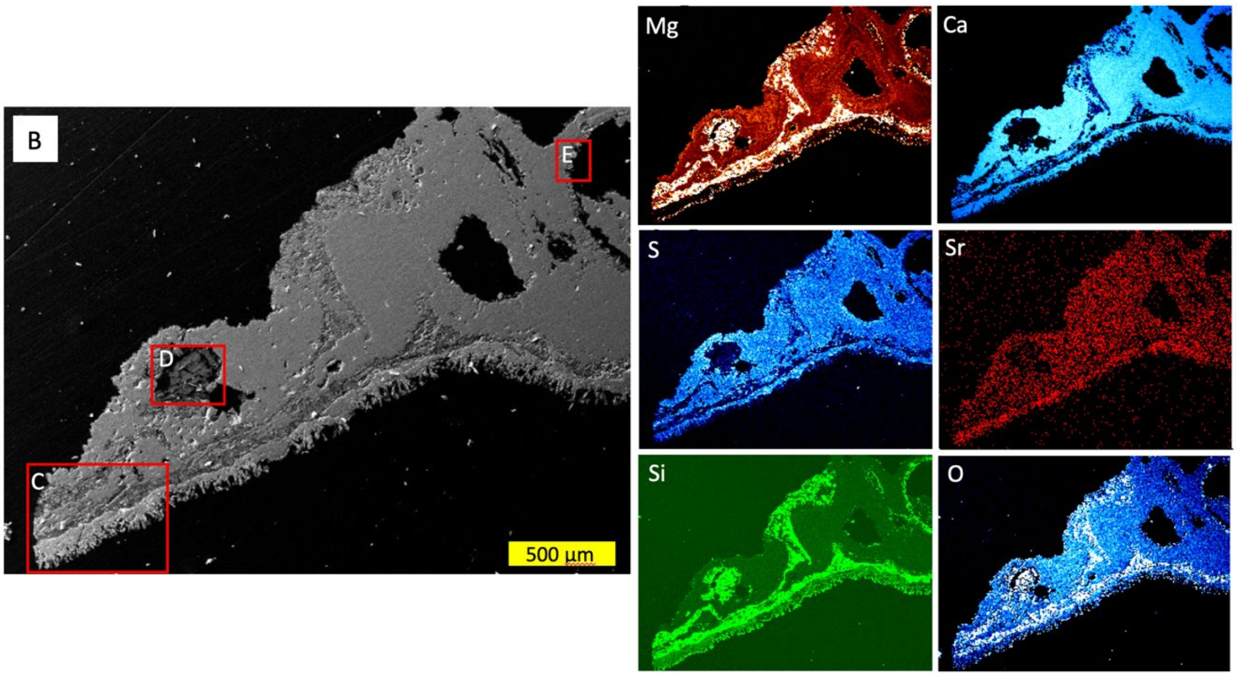

Figure 14. SEM image B and elemental distribution on the right side. Needle spar Crystal C, considered to be the stem cross section of plant fossils D, E.

Figure 15. SEM image of needle spar and elemental spectrum

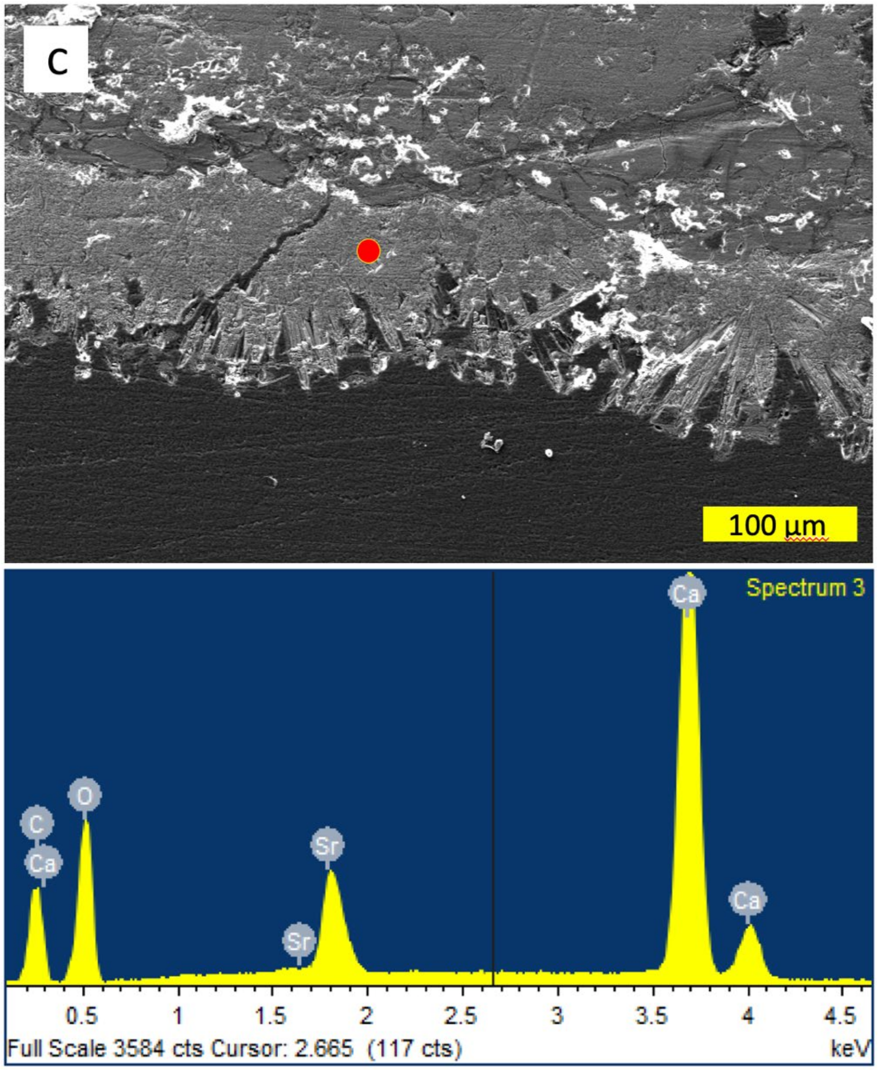

Figure 15. A graph showing the spectrum focusing on the needle spar.

Figure 16. Cross-section of plant fossil stem SEM image and elemental spectrum

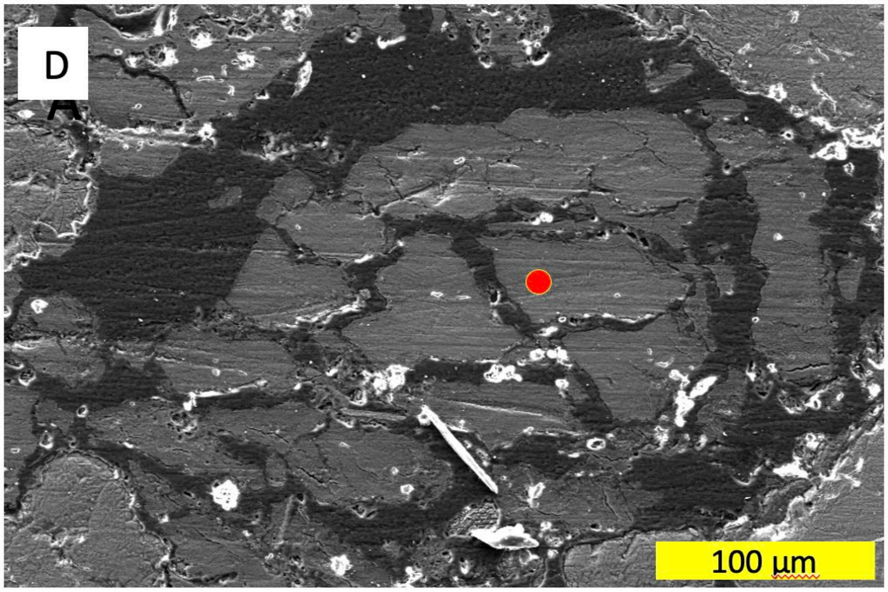

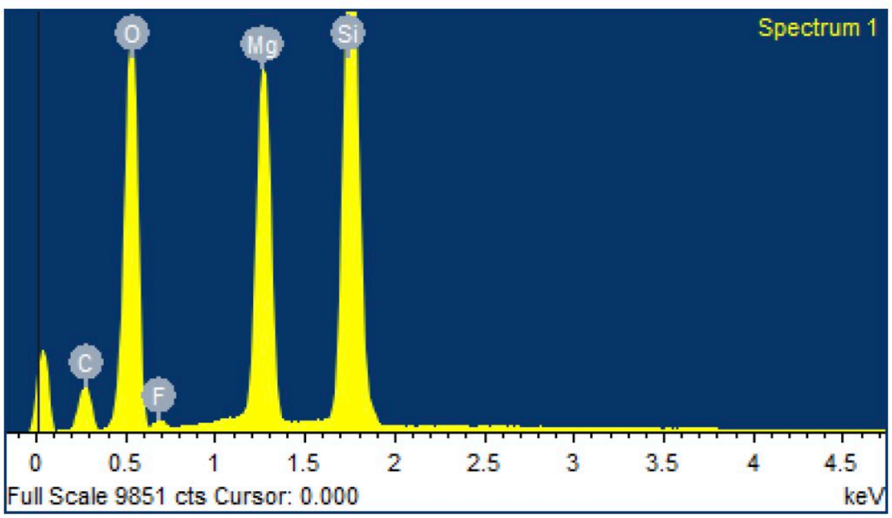

Figure 16. A graph showing the elemental spectrum focusing on the part that is considered to be the cross section of the stem of a plant.

Figure 17. SEM image and elemental distribution of KWST (plant cells)

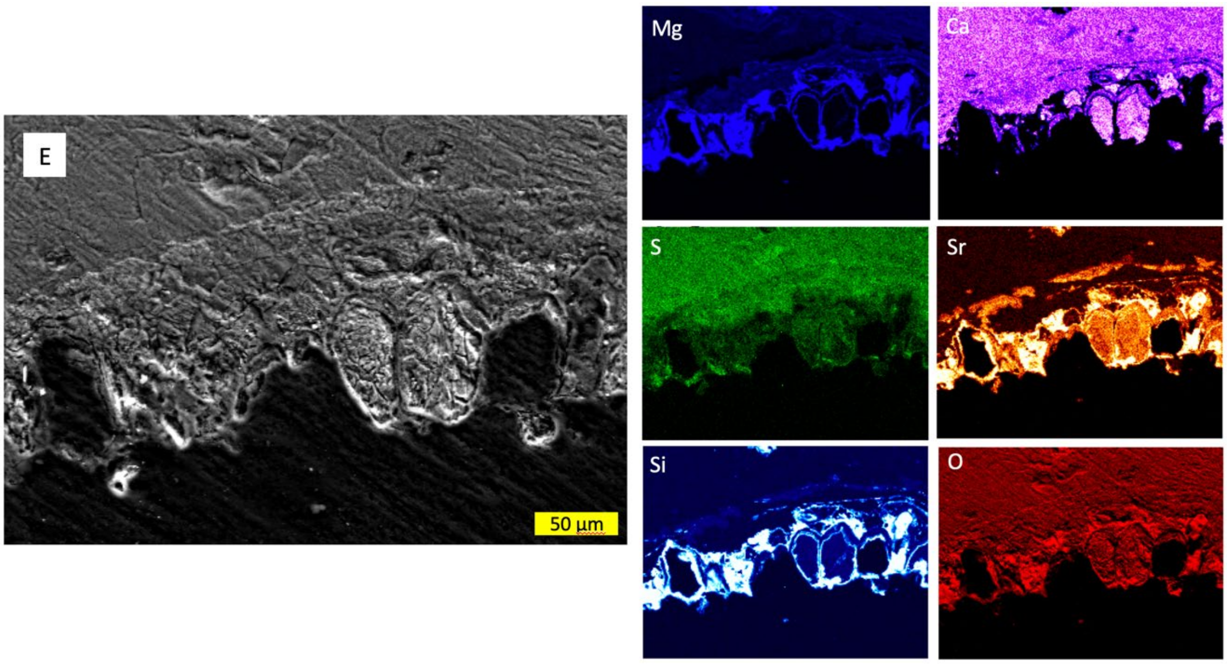

Figure 17. Elemental mapping of silicified plant (root) cells.

Figure 18. Cross-section of plant fossil SEM image and elemental spectrum

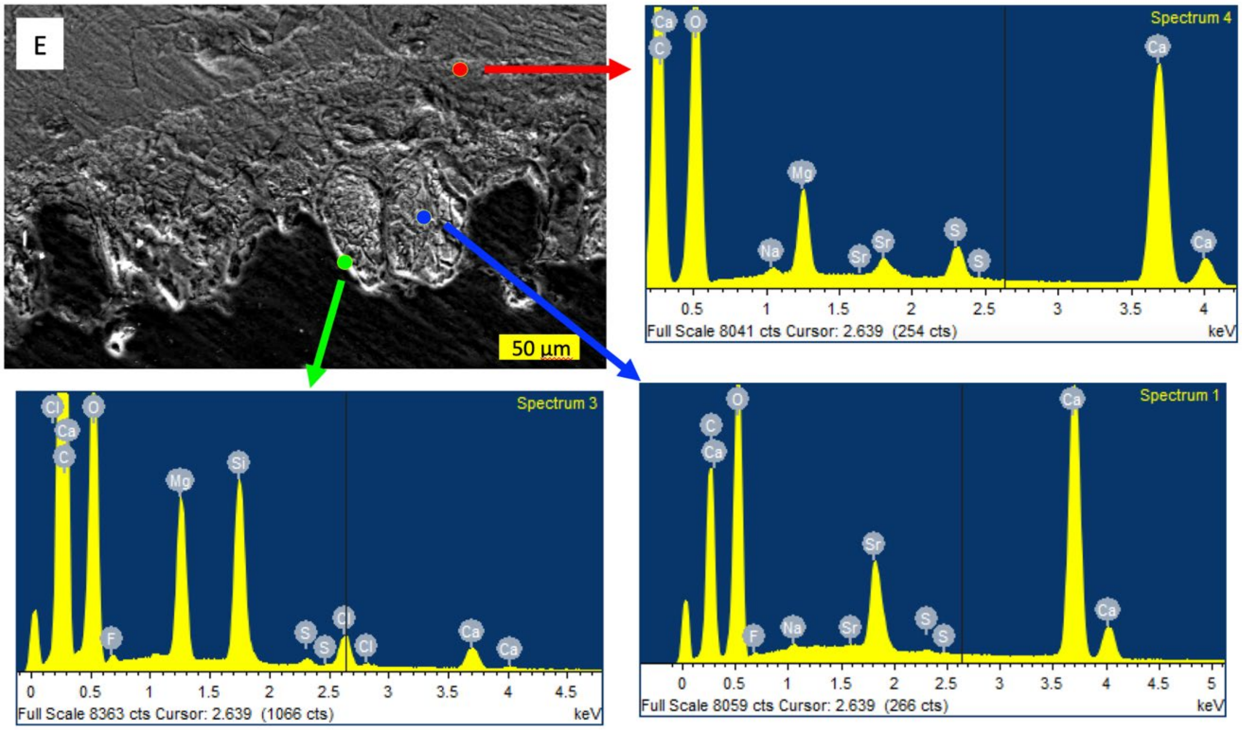

Figure 18. Graph of elemental measurement of each of the three parts that can be considered as plant cells.

Figure 19. Present-day and Quaternary lakes in Death Valley and adjacent areas

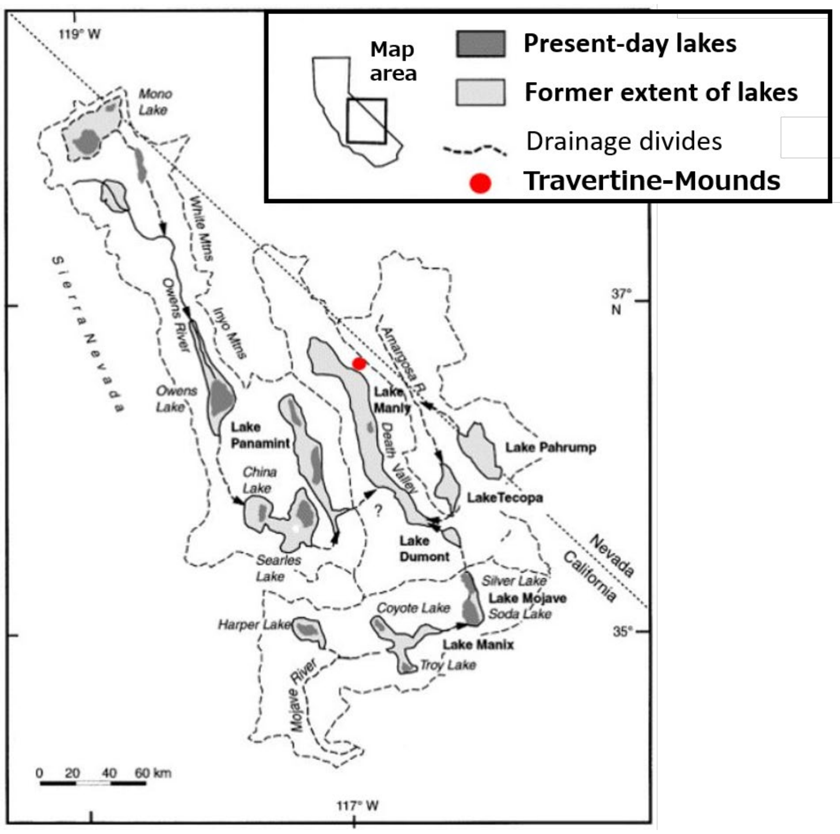

Figure 19. Present-day and Quaternary lakes in Death Valley and adjacent areas. The segment in dark gray shows present lakes, the light gray shows the former extent of lakes, and the red point denotes the Keane Wonder Mine Travertine mounds. Modified from V. P. Tchakerian et al, 2000.

Figure 20. Mammoth Hot Springs, Yellowstone National Park, Wyoming, U.S.A.

Figure 20. Calcite rafts from Mammoth Hot Springs, Yellowstone National Park, Wyoming, U.S.A. (image from Cook and Chafetz, 2017).

TABLES

Table 1. Point count data displayed as percentages for KWST site 2

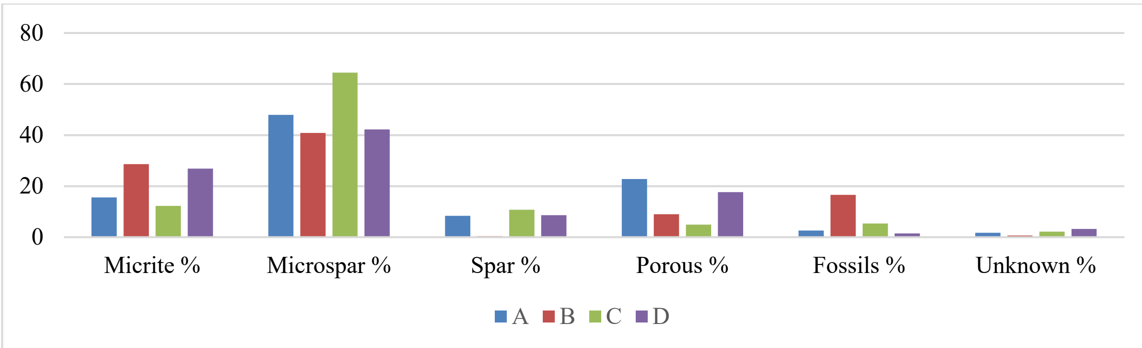

Table 1. Point counting data displayed as percentages for KWST sample 2 (A, B, C, D).

8. References

Aitken, M.J., 1998, An introduction to optical dating: Oxford, Oxford University Press.

Andrews, J.E., Riding, R., and Dennis, P.F., 1997, The stable isotope record of environmental and climatic signals in modern terrestrial microbial carbonates from Europe: Palaeogeography, Palaeoclimatology, Palaeoecology, v. 129, p. 171–189, doi:10.1016/S0031-0182(96)00120-4.

Arenas, C., and Jones, B., 2017, Temporal and environmental significance of microbial lamination: Insights from Recent fluvial stromatolites in the River Piedra, Spain: Sedimentology, v. 64, p. 1597–1629, doi:10.1111/sed.12365.

Armenteros, I., and Ghannem, N., 2021, A wet climatic terrestrial carbonate record in the middle-upper Pleistocene, north Tunisia: Facies, v. 67, p. 1–28, doi:10.1007/s10347-020-00612-x.

Bargar, K.E. Geology and Thermal History of Mammoth Hot Springs, YNP, WY:

Bedinger, M.S., and Harrill, J.R., 2012, Groundwater geology and hydrology of Death Valley National Park, California and Nevada: Natural Resources Technical Report NPS/NRSS/WRD/NRTR—2012/652, p. 117.

De Boever, E., Brasier, A.T., Foubert, A., and Kele, S., 2017, What do we really know about early diagenesis of non-marine carbonates? Sedimentary Geology, v. 361, p. 25–51, doi:10.1016/j.sedgeo.2017.09.011.

Chafetz, H.S., and Folk, R.L., 1984, BACTERIALLY CONSTRUCTED CONSTITUENTS l: v. 54.

Chafetz, H.S., and Guidry, S.A., 1999, Bacterial shrubs, crystal shrubs, and ray-crystal shrubs: Bacterial vs. abiotic precipitation: Sedimentary Geology, v. 126, p. 57–74, doi:10.1016/S0037-0738(99)00032-9.

Cook, B.I., Ault, T.R., and Smerdon, J.E., 2015, Unprecedented 21st century drought risk in the American Southwest and Central Plains: Science Advances, v. 1, p. 1–7, doi:10.1126/sciadv.1400082.

Cook, M., and Chafetz, H.S., 2017, Sloping fan travertine, Belen, New Mexico, USA: Sedimentary Geology, v. 352, p. 30–44, doi:10.1016/j.sedgeo.2017.02.010.

East, N., 2019, Climate-and Human-Induced Vegetation Changes in Northwestern Turkey Climate- and Human-Induced Vegetation Changes in Northwestern Turkey and the Southern Levant since the Last Glacial Dissertation Andrea Miebach aus Bergisch Gladbach:

De Filippis, L., Faccenna, C., Billi, A., Anzalone, E., Brilli, M., Özkul, M., Soligo, M., Tuccimei, P., and Villa, I.M., 2012, Growth of fi ssure ridge travertines from geothermal springs of Denizli Basin, western Turkey: Bulletin of the Geological Society of America, v. 124, p. 1629–1645, doi:10.1130/B30606.1.

Fouke, B.W., 2011, Hot-spring Systems Geobiology: Abiotic and biotic influences on travertine formation at Mammoth Hot Springs, Yellowstone National Park, USA: Sedimentology, v. 58, p. 170–219, doi:10.1111/j.1365-3091.2010.01209.x.

Gandin, A., and Capezzuoli, E., 2014, Travertine: Distinctive depositional fabrics of carbonates from thermal spring systems: Sedimentology, v. 61, p. 264–290, doi:10.1111/sed.12087.

GUO, L. et al., 2017, Sloping fan travertine, Belen, New Mexico, USA: Sedimentology, v. 352, p. 30–44, doi:10.1016/j.sedgeo.2017.02.010.

GUO, L., and RIDING, R., 1994, Origin and diagenesis of Quaternary travertine shrub fabrics, Rapolano Terme, central Italy: Sedimentology, v. 41, p. 499–520, doi:10.1111/j.1365-3091.1994.tb02008.x.

Hancock, P.L., Chalmers, R.M.L., Altunel, E., and C, Z., 1999, Travitonics : using travertines in active fault studies: v. 21, p. 903–916.

Hooke, R.L., 1999, Lake Manly(?) shorelines in the Eastern Mojave Desert, California: Quaternary Research, v. 52, p. 328–336, doi:10.1006/qres.1999.2080.

Ku, T.L., Luo, S., Lowenstein, T.K., Li, J., and Spencer, R.J., 1998, U-series chronology of lacustrine deposits in Death Valley, California: Quaternary Research, v. 50, p. 261–275, doi:10.1006/qres.1998.1995.

Lowenstein, T.K., Li, J., Brown, C., Roberts, S.M., Ku, T.L., Luo, S., and Yang, W., 1999, 200 k.y. paleoclimate record from Death Valley salt core: Geology, v. 27, p. 3–6, doi:10.1130/0091-7613(1999)027<0003:KYPRFD>2.3.CO;2.

Machette, M.N., Slate, J.L., and Phillips, F.M., 2008, Terrestrial cosmogenic-nuclide dating of alluvial fans in Death Valley, California: US Geological Survey Professional Paper, p. 1–39, doi:10.3133/pp1755.

Minissale, A., Kerrick, D.M., Magro, G., Murrell, M.T., and Paladini, M., 2002, Geochemistry of Quaternary travertines in the region north of Rome (Italy): structural , hydrologic and paleoclimatic implications: v. 203.

Van Noten, K., Topal, S., Baykara, M.O., Özkul, M., Claes, H., Aratman, C., and Swennen, R., 2019, Pleistocene-Holocene tectonic reconstruction of the Ballık travertine (Denizli Graben, SW Turkey): (De)formation of large travertine geobodies at intersecting grabens: Journal of Structural Geology, v. 118, p. 114–134, doi:10.1016/j.jsg.2018.10.009.

Owen, L.A., Frankel, K.L., Knott, J.R., Reynhout, S., Finkel, R.C., Dolan, J.F., and Lee, J., 2011, Beryllium-10 terrestrial cosmogenic nuclide surface exposure dating of Quaternary landforms in Death Valley: Geomorphology, v. 125, p. 541–557, doi:10.1016/j.geomorph.2010.10.024.

Özkul, M., Kele, S., Gökgöz, A., Shen, C.C., Jones, B., Baykara, M.O., Fórizs, I., Németh, T., Chang, Y.W., and Alçiçek, M.C., 2013, Comparison of the Quaternary travertine sites in the Denizli extensional basin based on their depositional and geochemical data: Sedimentary Geology, v. 294, p. 179–204, doi:10.1016/j.sedgeo.2013.05.018.

Pedley, M., 2009, Tufas and travertines of the Mediterranean region : a testing ground for freshwater carbonate concepts and developments: , p. 221–246, doi:10.1111/j.1365-3091.2008.01012.x.

Pentecost, A. Travertine:

Porta, G. Della, and Barilaro, F., 2012, Non-Marine Carbonate Precipitates : A Review Based on Recent and Ancient Case Studies: AAPG International Conference and Exhibition, v. 30217, p. 40.

Della Porta, G., Croci, A., Marini, M., and Kele, S., 2017, Depositional architecture, facies character and geochemical signature of the Tivoli travertines (pleistocene, acque albule basin, central Italy): Rivista Italiana di Paleontologia e Stratigrafia, v. 123, p. 487–540, doi:10.13130/2039-4942/9148.

Rhodes, E.J., 2011, Optically Stimulated Luminescence Dating of Sediments over the Past 200,000 Years: Annual Review of Earth and Planetary Sciences, v. 39, p. 461–488, doi:10.1146/annurev-earth-040610-133425.

Ricketts, J.W., Ma, L., Wagler, A.E., and Garcia, V.H., 2019, Global travertine deposition modulated by oscillations in climate: Journal of Quaternary Science, v. 34, p. 558–568, doi:10.1002/jqs.3144.

Sant'Anna, L.G., Riccomini, C., Rodrigues-Francisco, B.H., Sial, A.N., Carvalho, M.D., and Moura, C.A.V., 2004, The Paleocene travertine system of the Itaboraí basin, Southeastern Brazil: Journal of South American Earth Sciences, v. 18, p. 11–25, doi:10.1016/j.jsames.2004.08.005.

Seager, R., Neelin, D., Simpson, I., Liu, H., Henderson, N., Shaw, T., Kushnir, Y., Ting, M., and Cook, B., 2014, Dynamical and thermodynamical causes of large-scale changes in the hydrological cycle over North America in response to global warming: Journal of Climate, v. 27, p. 7921–7948, doi:10.1175/JCLI-D-14-00153.1.

Steinkampf, W.C. et al., 1999, 200 k.y. paleoclimate record from Death Valley salt core: Bulletin of the Geological Society of America, v. 57, p. 173–176, doi:10.1130/0091-7613(1999)027<0003:KYPRFD>2.3.CO;2.

Steinkampf, W.C., and Werrell, W.L., 2001, Ground-Water Flow to Death Valley, as Inferred from the Chemistry and Geohydrology of Selected Springs in Death Valley National Park , California and Nevada: US Geological Survey Water-Resources Investigations Report 98-4114, p. 37.

Su, J. et al., 2020, Chesapeake Bay acidification buffered by spatially decoupled carbonate mineral cycling: Nature Geoscience, v. 13, p. 441–447, doi:10.1038/s41561-020-0584-3.

Takashima, C., and Kano, A., 2005, Depositional processes of travertine developed at Shionoha hot spring, Nara Prefecture, Japan: The Journal of the Geological Society of Japan, v. 111, p. 751–764, doi:10.5575/geosoc.111.751.

Toker, E. et al., 2017, Sloping fan travertine, Belen, New Mexico, USA: Sedimentology, v. 352, p. 30–44, doi:10.1016/j.sedgeo.2017.02.010.

Toker, E., Kayseri-Özer, M.S., Özkul, M., and Kele, S., 2015, Depositional system and palaeoclimatic interpretations of Middle to Late Pleistocene travertines: Kocabaş, Denizli, south-west Turkey: Sedimentology, v. 62, p. 1360–1383, doi:10.1111/sed.12186.

Troxel, B.W., and Wright, L.A., 1989, Geologic map of the central and northern Funeral Mountains and adjacent areas, Death Valley region, Southern California:

Wendt, K.A., Pythoud, M., Moseley, G.E., Dublyansky, Y. V., Edwards, R.L., and Spötl, C., 2020, Paleohydrology of southwest Nevada (USA) based on groundwater 234U/238U over the past 475 k.y.: Bulletin of the Geological Society of America, v. 132, p. 793–802, doi:10.1130/B35168.1.

Yao, J., Liu, H., Huang, J., Gao, Z., Wang, G., Li, D., Yu, H., and Chen, X., 2020, Accelerated dryland expansion regulates future variability in dryland gross primary production: Nature Communications, v. 11, p. 1–10, doi:10.1038/s41467-020-15515-2.